Supporting Information

New Orientation: A Downward-pointing Vertical Inductively Coupled Plasma Mass Spectrometer for the Analysis of Microsamples

Thomas Vonderach, Bodo Hattendorf and Detlef Günther*

Laboratory of Inorganic Chemistry, Department of Chemistry and Applied Biosciences, ETH Zurich, Vladimir-Prelog-Weg 1, 8093 Zurich, Switzerland

*Corresponding author

E-mail: detlef.guenther@sl.ethz.ch

Table of Contents

Experimental Section

Cooling Plates. A new cooling system was designed in order to protect the torch box or its inner parts from damage by the ascending heat from the ICP. It was equipped with two actively cooled and one passively cooled metal plates, the latter being oriented perpendicular to the torch axis and placed above the induction coil as shown in the rendering in **Figure S1**. The two actively cooled plates were equipped with milled cooling loops through which a continuous flow of coolant was pumped. The vertical metal plate shield was screwed onto the two actively cooled metal plates to ensure efficient heat dissipation and that the torch box temperature remained below 50° C.

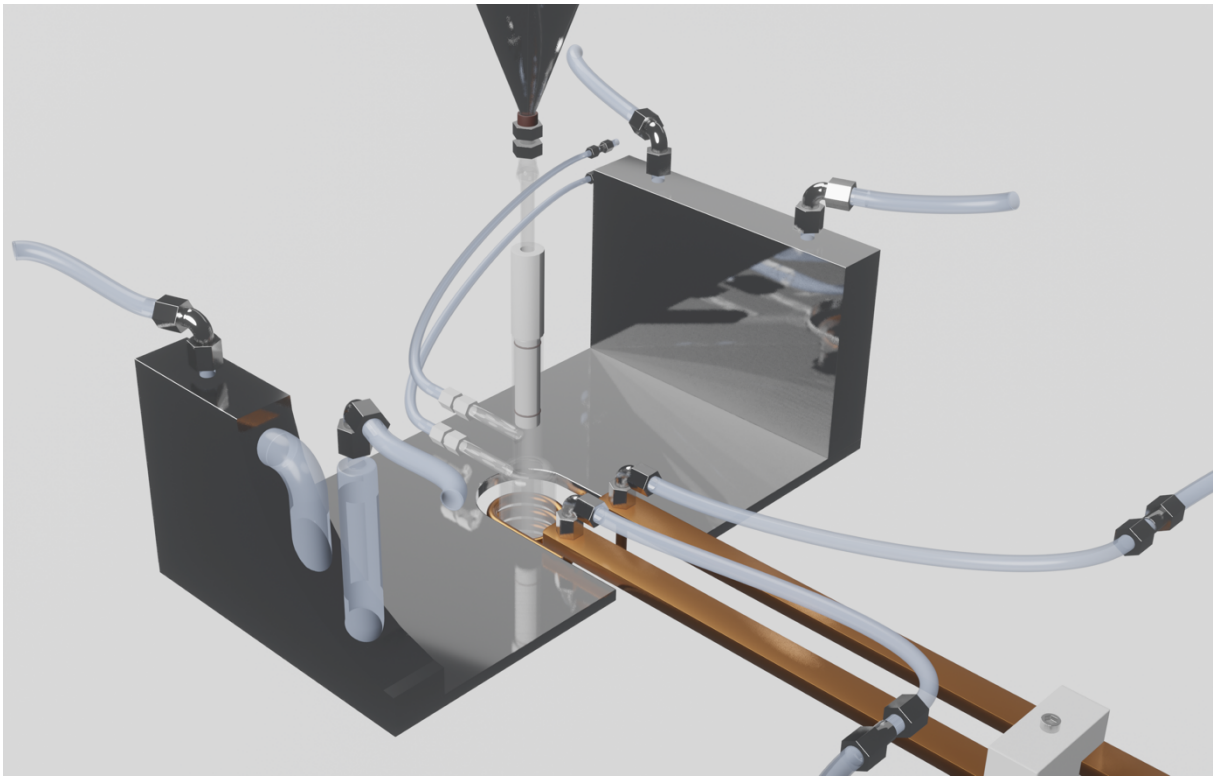

Figure S1 Rendering of the in-house designed and constructed torch box cooling system.

Sample Preparation. A multi-element solution was prepared in 1% HNO_3 using ICP reference standards (Inorganic Ventures and Merck), high purity water (18.2 MΩ cm, Millipore) and sub-boiled HNO_3. The solution contained Li, Na, Mg, Co, Y, Rh, Ag, In, Cs, Ce, Eu, Ho, Lu, Ir, Pb, Bi, U at a concentration of 20 μg L^{-1}. EQ4 calibration beads (EQ4_P13H2302, Fluidigm) suspended in high purity water comprising a particle number concentration (PNC) of 3.3 x 10^5 beads $(mL)^{-1}$ were analyzed directly without any further sample preparation. The used polymer microbeads contained ^{140}Ce (2 x 10^7 ± 15% atoms per bead), ^{153}Eu (1.2 x 10^7 ± 15% atoms per bead), ^{165}Ho (7.6 x 10^6 ± 15% atoms per bead), ^{175}Lu (9.8 x 10^6 ± 15% atoms per bead) according to the Certificate of Analysis (COA002 V4 Dec 2013) provided by DVS Sciences. The beads further contained ^{142}Ce, ^{151}Eu and ^{176}Lu isotopes, which were not investigated within the presented study.

Sample Introduction. Monodisperse droplets were generated using commercially available microdroplet generators (MDG, Microdroplet dispenser MD-K-150/17 & Autodrop Pipette AD-KH-501/0108, microdrop GmbH, Germany). This type of MDG is equipped with a piezoelectrically actuated quartz capillary that possesses a specified inner nozzle diameter (30 and 50 μm). The size, velocity and stability of the ejected droplets depend on the voltage pulses, *i. e.* amplitude and duration. The droplet sizes in single pulse mode measured approximately 45 and 65 μm. The Microdrop Dispensing System (MD-E-3000, microdrop GmbH, Germany) was used to generate droplets at dispensing frequencies between 20-1000 Hz. The MDG was mounted in a 3D-printed holder, equipped with two windows allowing the observation of the ejected droplets at the dispenser nozzle tip. [1] The droplets are monitored by stroboscopic illumination and a CCD camera. The open source software ImageJ (W. S. Rasband, US National Institutes of Health, Bethesda, MD, USA) was used for further image processing and the determination of the droplet size. The uncertainty of the determined droplet sizes was estimated to be 1.4 μm given by the size of a single pixel. Helium was added upstream of the MDG nozzle via a port that was positioned 5 cm above the tip. The MDG holder was mounted on an in-house developed coaxial flow adapter that was equipped with four argon ports. The droplet delivery system had a fall distance of approximately 28 cm between the capillary nozzle of the dispenser and the plasma. In a second approach, the short glass tube between the coaxial flow adapter and the injector was replaced by a gas-exchange-device (GED)[2]. The GED was employed to

further reduce the droplets' size and to minimize the amount of solvent entering the plasma. This configuration extended the falling distance by approximately 40 cm giving a total length of 68 cm.

Data Acquisition and Processing. To study the performance of the downward-pointing ICPMS different parameters and configurations were tested. **Table S1** summarizes the conditions used for various experiments, *e. g.* 0.9 and 1.8 mm injector diameter, approximately 65 μm and approximately 45 μm droplet sizes, with and without the GED as desolvation device, respectively.

The data were acquired using the Elan 3.5 software (PE/Sciex). The mass spectrometer was operated in single point peak-hopping mode, a dwell time of 100 ms and a settling time of 3 ms. In this mode ion signals from multiple droplets were averaged and the mean signal intensity was recorded for a total sampling time of one minute. A blank solution was measured for each experiment and its signal intensity was subtracted from the gross sample signal intensity. Furthermore, a correction to account for the variation of the mean droplet sizes was applied. Cs was added as droplet tracer also to the blank solution and used for optimization.

Mean droplet signals were acquired with and without using the GED for two different droplet sizes and injector diameters. The operating conditions are given in **Table S1.** The calculated detection efficiencies are presented in **Figure 2** and **Figure S4.**

In contrast to the acquisition mode as described above, polymer microbeads were analyzed for their Ce, Eu, Ho and Lu content using a dwell time of 20 ms and a settling time of 200 μs.

Data analysis was performed in OriginPro 2019 Version 9.6. The plots were generated using Python 3.7.

Summary of the Operating Conditions. **Table 1** was supplemented with the Auto Lens calibration parameters and the operating conditions for the experiments where a 0.9 mm injector was used were added.

	RF power [W]	He flow [L min^{-1}]	Ar flow [L min^{-1}]	aux gas flow [L min^{-1}]	plasma gas flow [L min^{-1}]	GED sweep gas flow [L min^{-1}]	sampling depth [mm]	droplet size [μm]	auto lens slope [V (amu)$^{-1}$]	auto lens intercept [V]	oxide ratio CeO/Ce [%]
∅ 1.8 mm injector											
MDG_45	800	0.41	0.32	1.5	13	-	11	47.1 ± 1.4	0.032	2.80	0.6
MDG_65	600	0.33	0.07	1.5	11	-	11	65.5 ± 1.4	0.039	1.70	2.6
MDG_45_GED	850	0.65	0.22	1.5	13	10.0	11	41.9 ± 1.4	0.011	3.70	0.2
MDG_65_GED	600	0.42	0.05	1.6	12	10.5	11	65.2 ± 1.4	0.015	2.77	0.5
MDG_65_GED	1300	0.16	0.04	0.9	15	9.0	11	65.8 ± 1.4	0.023	3.68	0.1
∅ 0.9 mm injector											
MDG_45	700	0.52	0.1	1.2	13	-	11	46.5 ± 1.4	0.033	2.50	0.4
MDG_65	550	0.12	0.05	1.6	11	-	11	65.1 ± 1.4	0.026	2.59	0.9
MDG_45_GED	1200	0.68	0.2	1.2	11	8.8	11	44.4 ± 1.4	0.017	3.46	0.2
MDG_65_GED	800	0.37	0.02	1.6	11	9.4	11	65.1 ± 1.4	0.030	2.80	0.3

Table S1 Summary of the operating conditions applied for the different experiments. Note that the plasma was optimized in a broad range of plasma power and gas flow conditions. A microdroplet generator (MDG) produced droplets in the size of approximately 45 or 65 μm that were either directly introduced into the ICP or partially desolvated using a gas-exchange device (GED). The slope and intercept obtained from the Auto Lens calibration was added.

A smaller slope, corresponds to a lower initial kinetic ion energy and thus lower bulk gas temperature in the ICP, while the intercept is considered to correspond to the plasma potential. There is no obvious correlation between the operating conditions and the bulk gas temperature. The highest bulk gas temperature for example would have been present when using only 600 W RF power and 0.07 L min^{-1} Ar + 0.33 L min^{-1} He carrier gas flow rates (MDG_65, 1.8 mm injector). In this case however the CeO^+/Ce^+ intensity ratio was far higher than for example when using the GED for desolvation (MDG_65_GED) where apparently a lower bulk gas temperature was obtained but a lower CeO^+/Ce^+ ratio could be achieved. These observations indicate that there is a

substantial difference between the bulk plasma properties and the conditions prevailing in the vicinity of the droplet (local temperature and oxygen partial pressure). While the bulk plasma seems to be hotter in the first case, local cooling and higher availability of oxygen from the solvent appear to prevent a similarly efficient dissociation of the refractory compounds.

Schematic Drawing of the Downward-Pointing ICPMS Prototype + GED. Before the droplets entered the plasma, they were guided through a so-called gas-exchange device (GED)[3], which served as a desolvation device. During transportation the droplets undergo a desolvation process and get reduced in size. The GED enables a gas exchange where the carrier gas (mixture of He and Ar) and the present solvent vapor gets exchanged by dry Ar. We expect that sweep gas adds partially to the total amount of carrier gas that is used to transport the droplets.

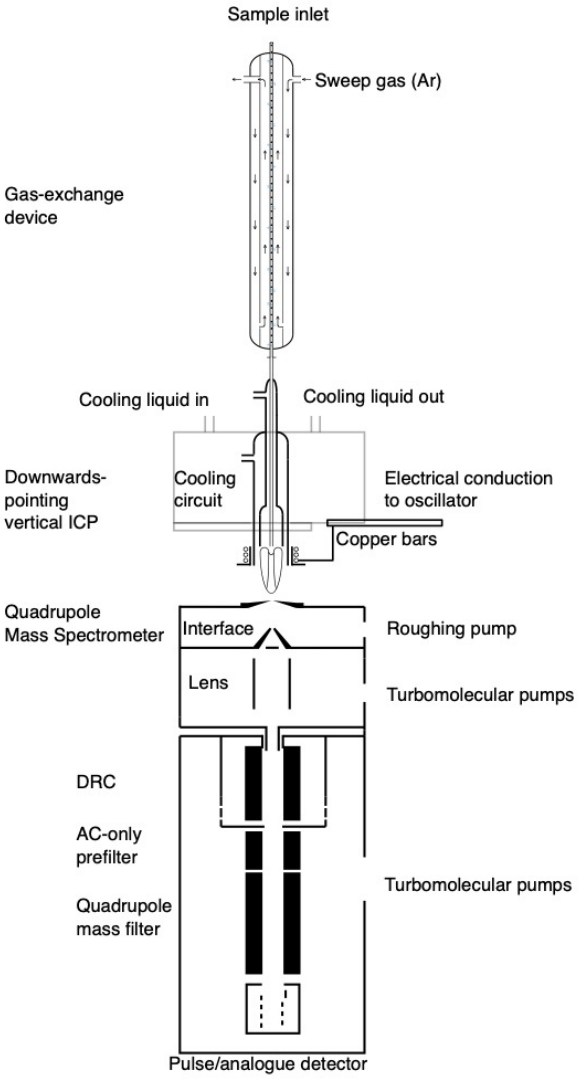

Figure S2 Schematic drawing of the downward-pointing ICPMS prototype highlighting the GED as a desolvation device mounted on top of the injector. Usually, a flow rate of 8-10 L min^{-1} of Ar was used as sweep gas. (see **Table S1**)

Results and Discussion

Ionization Potential and Heat of Vaporization Correlated with DEs.

The measured detection efficiencies in **Figure 2** were correlated with the element-specific ionization potential[4] and heat of vaporization[5, 6], respectively.

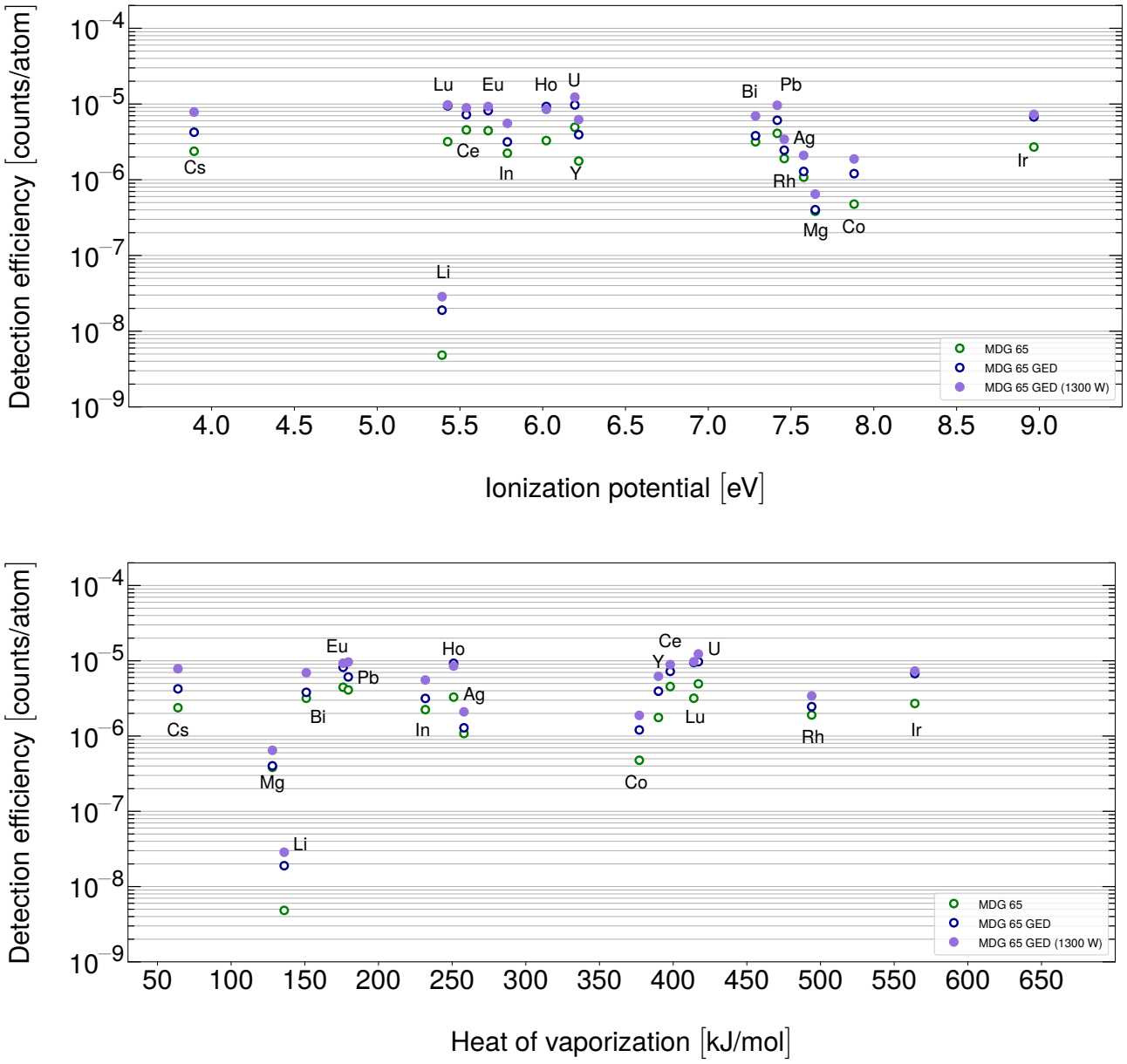

Figure S3 65 μm sized monodisperse droplets comprising a multi-element solution (20 ppb in 1% HNO_3) were analyzed. Further experimental conditions are provided in **Table S1**. The observed detection efficiencies (see **Figure 2**) were correlated with the element-specific ionization potential[4] and heat of vaporization[5, 6]. For the investigated elements, no significant differences between high and low power experiments were observed. (compare Tanner[7]) In contrast to the observations by Tanner [7], the low ICP power and low gas flow conditions adjusted on the downward-pointing plasma are not actually resulting in cold plasma conditions. (see also Auto lens calibration parameters

in **Table S1**). Note that the here reported heat of vaporization values are specific for the element present in its elemental state, *i. e.* in the ground state. However, due to the conditions in the plasma, the elements are present in the form of other species such as oxide species and therefore other heat of vaporization values are to be expected.

Detection Efficiencies – Using a 0.9 mm Injector. Analogously to the data presented in **Table 1** and **Figure 2**, the experiments were repeated after replacing the 1.8 mm injector by a 0.9 mm injector. The operating conditions are given in **Table S1.**

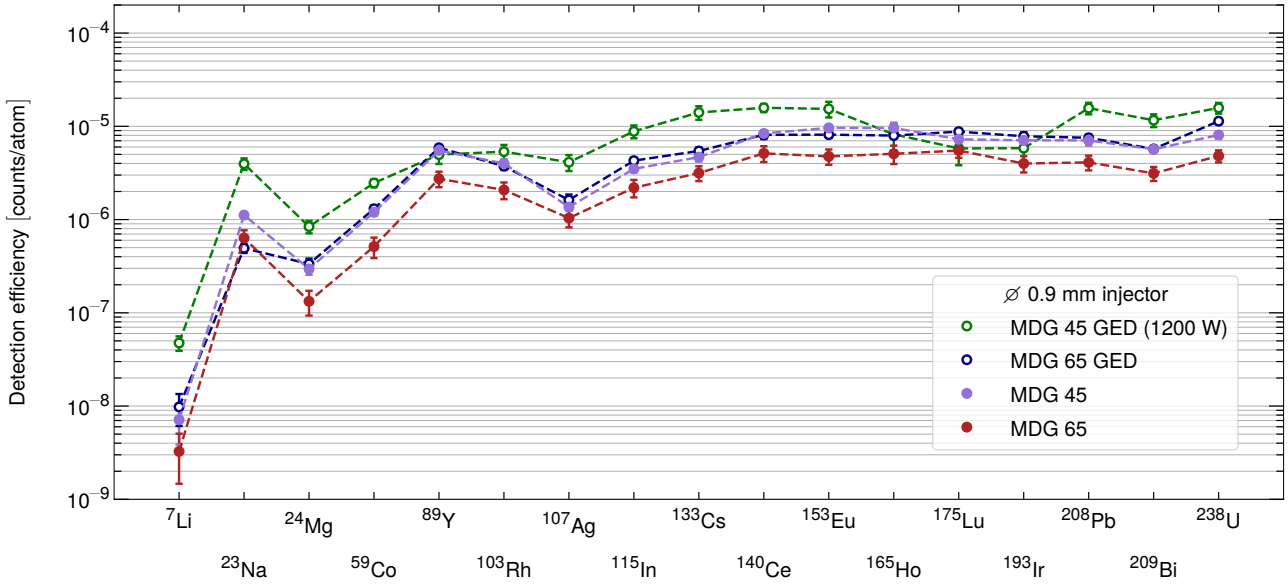

Figure S4 Detection efficiencies for various isotopes were determined using a 0.9 mm injector. Significantly different optimization parameters compared to standard operating conditions were applied (**Table S1**), and yet similar, *i. e.* instrument type specific, DEs were obtained in the presented experiments even for different droplet sizes, with and without desolvation or low and high ICP power.

Single Microbead Detection – Via Monodisperse Droplets.

EQ4 calibration beads (EQ4_P13H2302, Fluidigm) suspended in high purity water comprising a particle number concentration (PNC) of 3.3 x 10^5 beads $(mL)^{-1}$ were analyzed via monodisperse droplets. The polymer microbeads contained ^{140}Ce (2 x 10^7 ± 15% atoms per bead), ^{153}Eu (1.2 x 10^7 ± 15% atoms per bead), ^{165}Ho (7.6 x 10^6 ± 15% atoms per bead), ^{175}Lu (9.8 x 10^6 ± 15% atoms per bead) according to the Certificate of Analysis (COA002 V4 Dec 2013) provided by DVS Sciences.

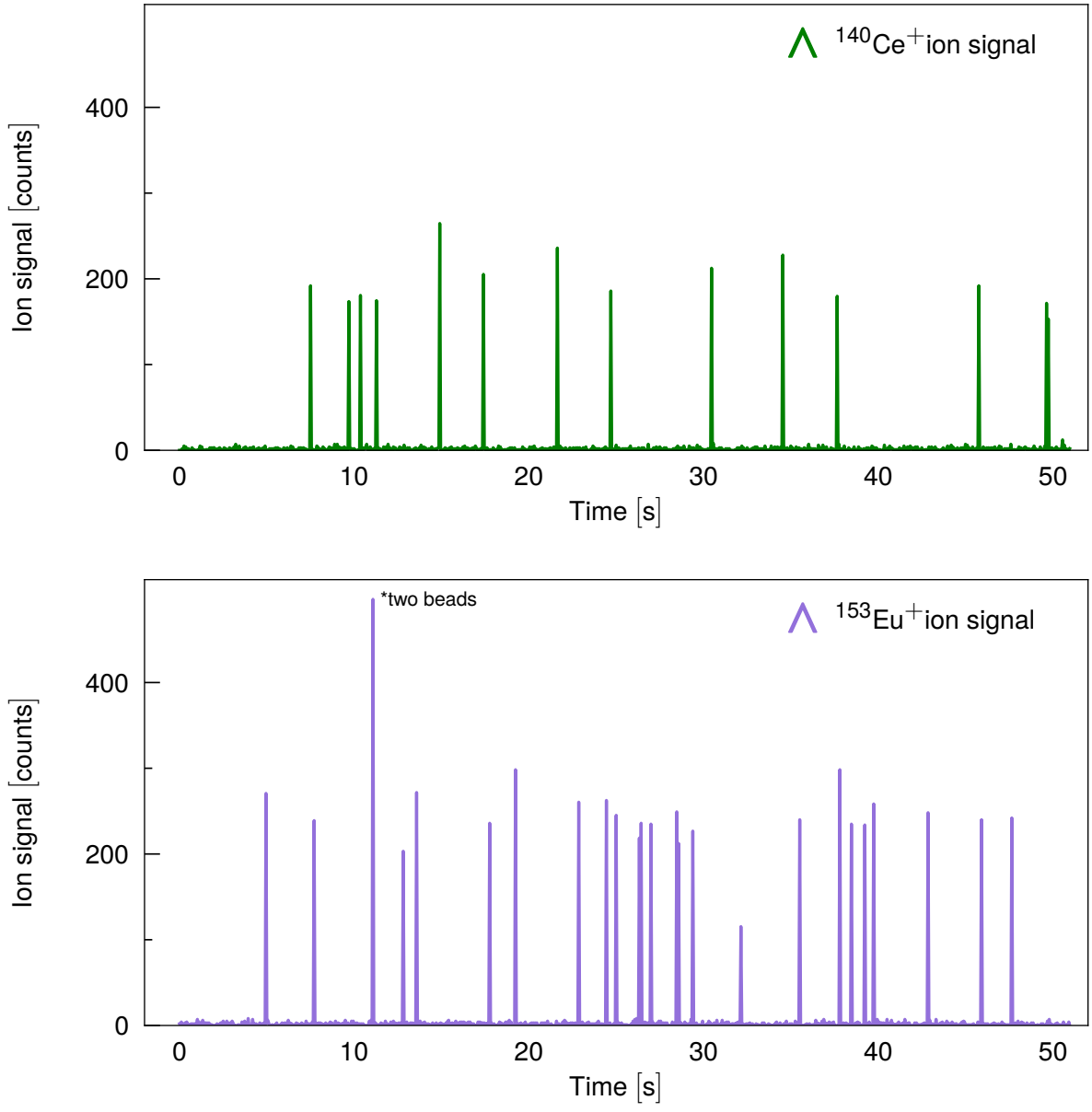

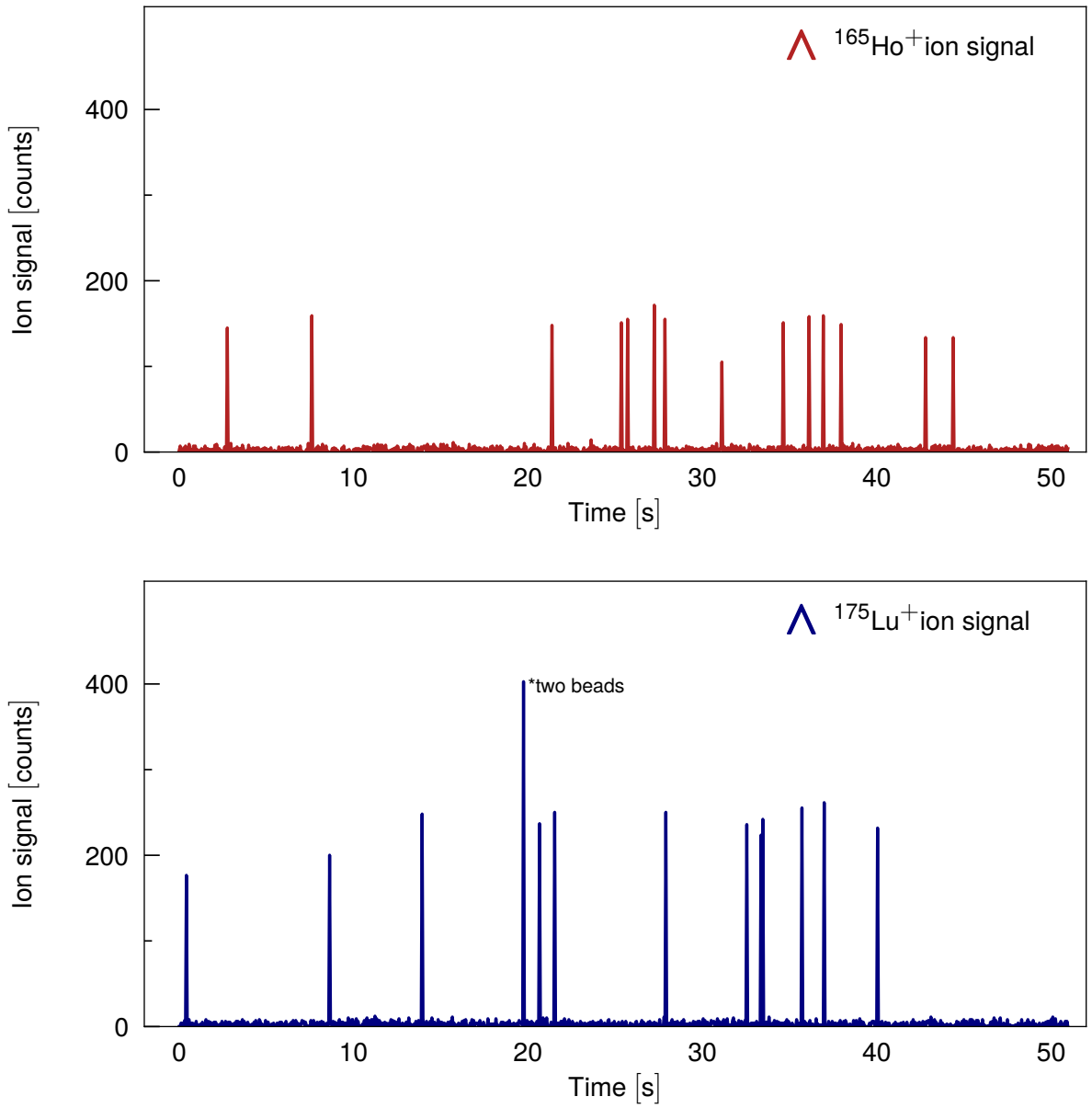

Figure S5 Time-resolved ion signals indicating the detection of the polymer microbeads are shown. $^{133}Cs^{+}$ (droplet tracer), $^{140}Ce^{+}$, $^{153}Eu^{+}$, $^{165}Ho^{+}$, $^{175}Lu^{+}$ ion signals were acquired using peak hopping mode at a dwell time of 10 ms for each analyte. The following operating conditions were applied: 0.07 L min^{-1} Ar and 0.39 L min^{-1} He carrier gas, 600 W ICP power, 10 L min^{-1} Ar sweep gas, 10 L min^{-1} plasma gas, 2 L min^{-1} auxiliary gas, 11 mm sampling depth (below load coil), 1.8 mm injector; the lens voltages were optimized individually: ^{140}Ce and ^{153}Eu @ lens voltage 3.5 V; ^{165}Ho and ^{175}Lu @ 3.75 V; dispensing frequency 50 Hz. On average, we obtained DEs of 9.9 x 10^{-6} for $^{140}Ce^{+}$, 2.1 x 10^{-5} for $^{153}Eu^{+}$, 2 x 10^{-5} for $^{165}Ho^{+}$ and 2.5 x 10^{-5} for $^{175}Lu^{+}$.

Single Microbead Detection – Via Nebulizer and Spray Chamber.

EQ4 calibration beads (EQ4_P13H2302, Fluidigm) suspended in high purity water comprising a particle number concentration (PNC) of 3.3 x 10^5 beads $(mL)^{-1}$ were analyzed under standard conditions using a concentric nebulizer (PFA, Microflow, 100-1843) and a cyclonic spray chamber (quartz, AHF). The same batch of polymer microbeads as described in the paragraph above was used for this experiment. The polymer microbeads contained ^{140}Ce (2 x 10^7 ± 15% atoms per bead), ^{153}Eu (1.2 x 10^7 ± 15% atoms per bead), ^{165}Ho (7.6 x 10^6 ± 15% atoms per bead), ^{175}Lu (9.8 x 10^6 ± 15% atoms per bead) according to the Certificate of Analysis (COA002 V4 Dec 2013) provided by DVS Sciences.

(a)

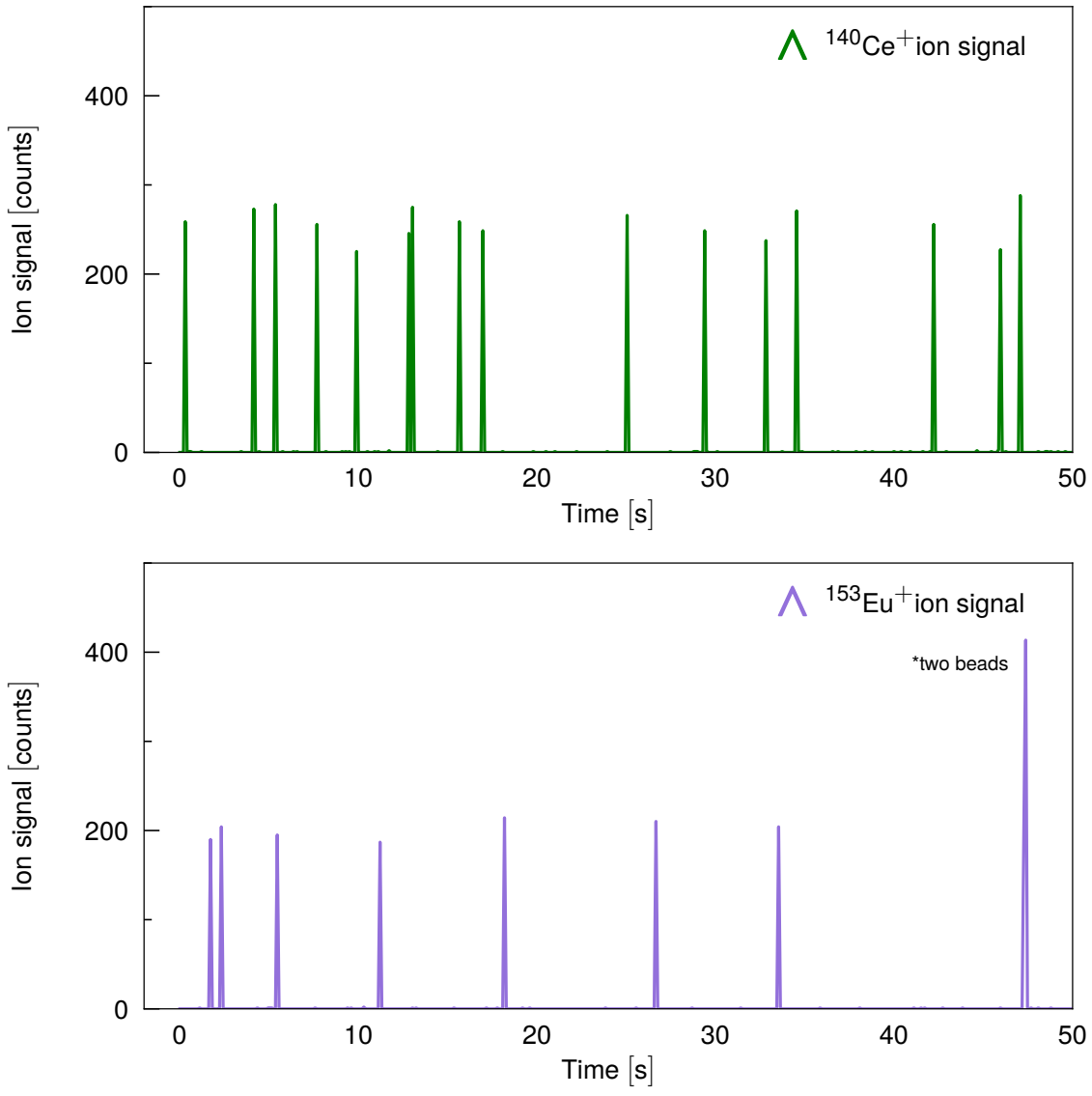

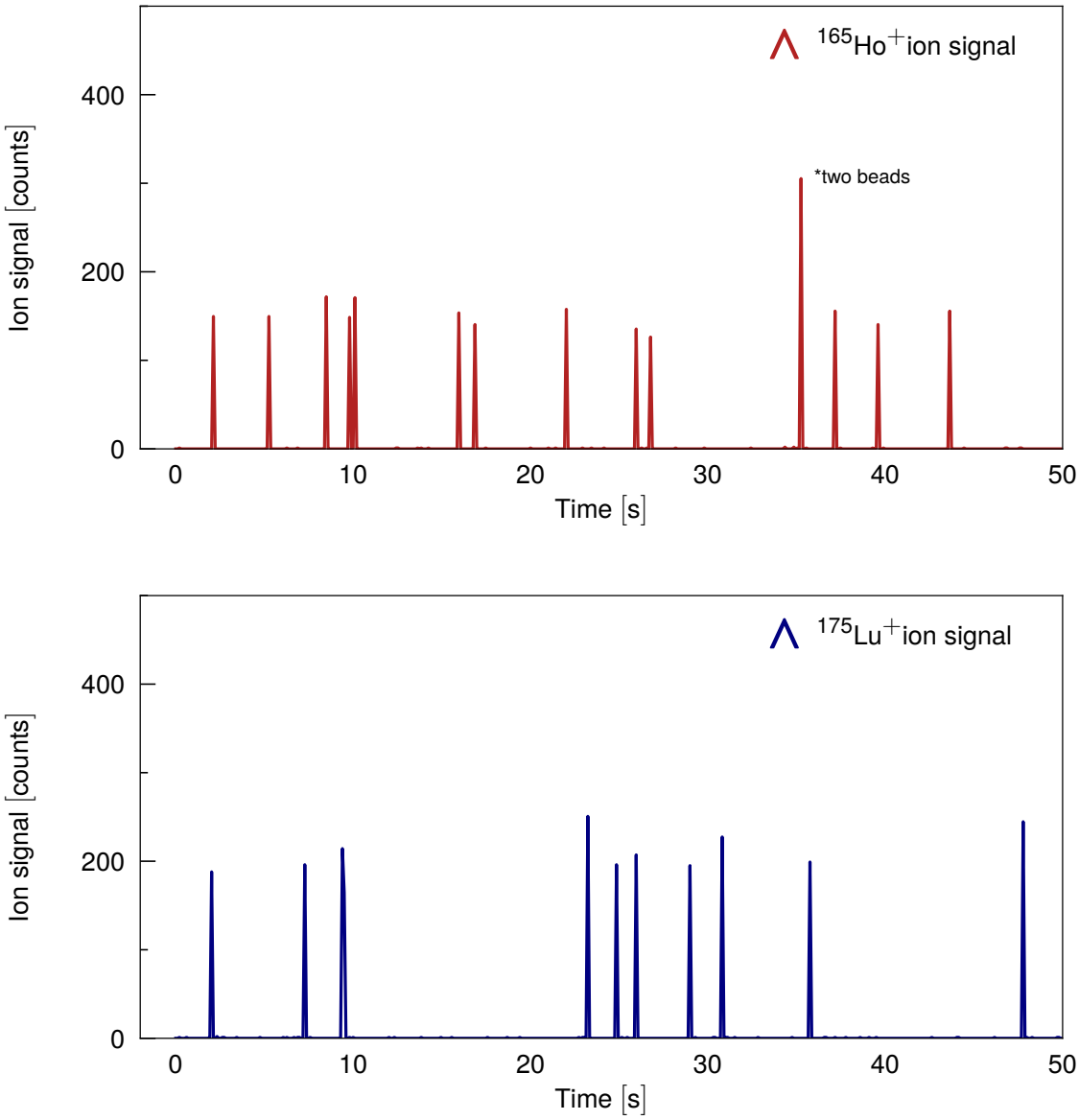
$^{165}Ho^{+}$ion signal
*two beads
Ion signal [counts]
Time [s]
0
200
400
0
10
20
30
40
50
$^{175}Lu^{+}$ion signal
Ion signal [counts]
Time [s]
0
200
400
0
10
20
30
40
50

(b)

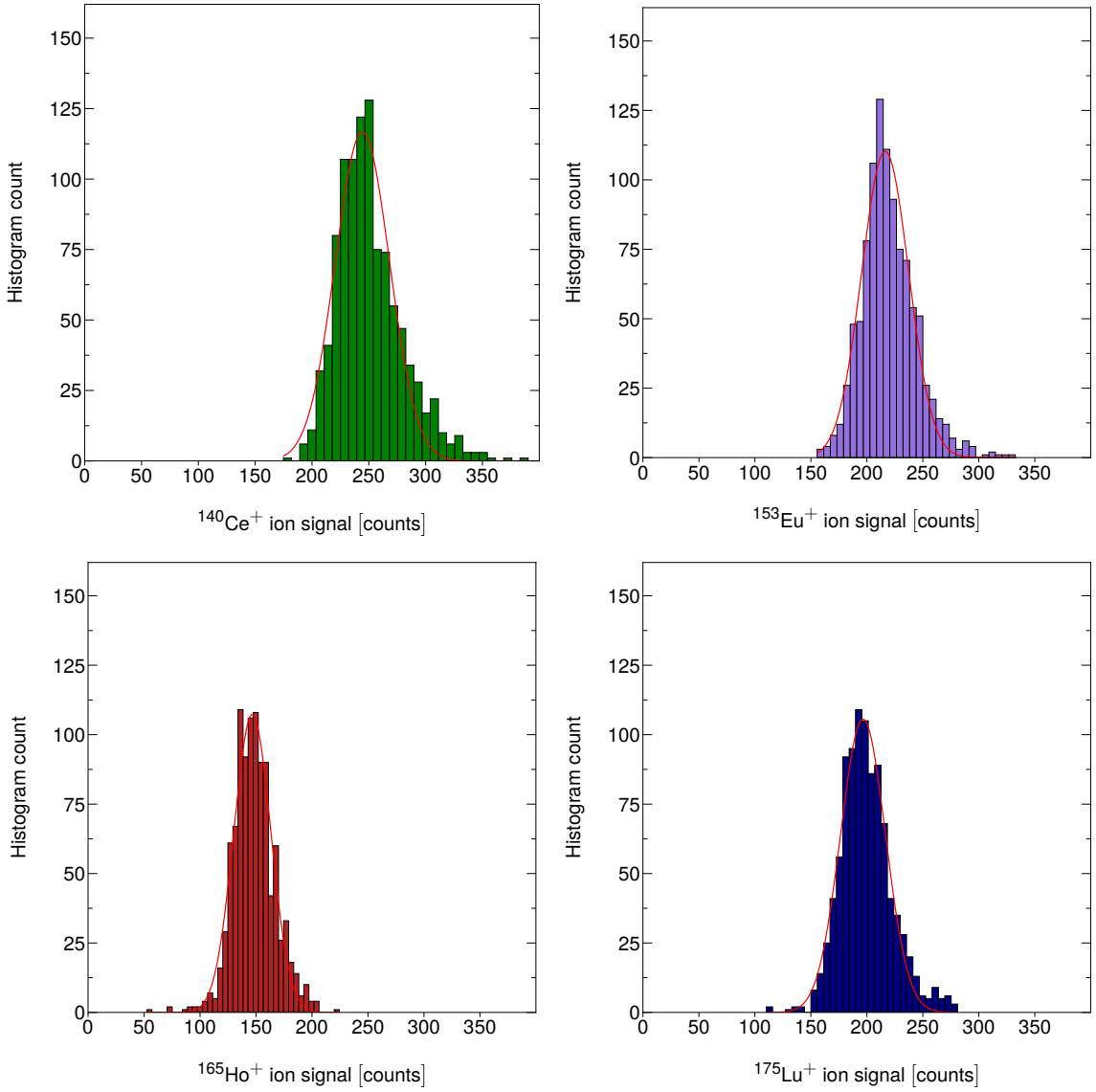

Figure S6 EQ4 calibration beads (EQ4_P13H2302, Fluidigm) suspended in high purity water comprising a particle number concentration (PNC) of 3.3 x 10^5 beads $(mL)^{-1}$ were analyzed using a concentric nebulizer (PFA, Microflow, 100-1843) and a cyclonic spray chamber (quartz, AHF). The following operating conditions were applied: 0.83 L min^{-1} Ar nebulizer/carrier gas, 1400 W ICP power, 15 L min^{-1} plasma gas, 0.66 L min^{-1} auxiliary gas, 11 mm sampling depth, 1.8 mm injector; the lens voltages were optimized using the Auto-Lens calibration. Prior analysis the bead suspension was diluted by a factor of 10 using high purity water. Time-resolved ion signals are shown in (a) and the signal distributions (histograms) are given in (b). The following DEs were obtained: 1.2 x 10^{-5} for $^{140}Ce^{+}$, 1.8 x 10^{-5} for $^{153}Eu^{+}$, 1.9 x 10^{-5} for $^{165}Ho^{+}$ and 2 x 10^{-5} for $^{175}Lu^{+}$.

Falling Tube Setup – Limited Throughput.

The capabilities of the falling tube setup[1, 8] were tested analyzing 68 μm sized monodisperse droplets and the results are presented in **Figure S7**.

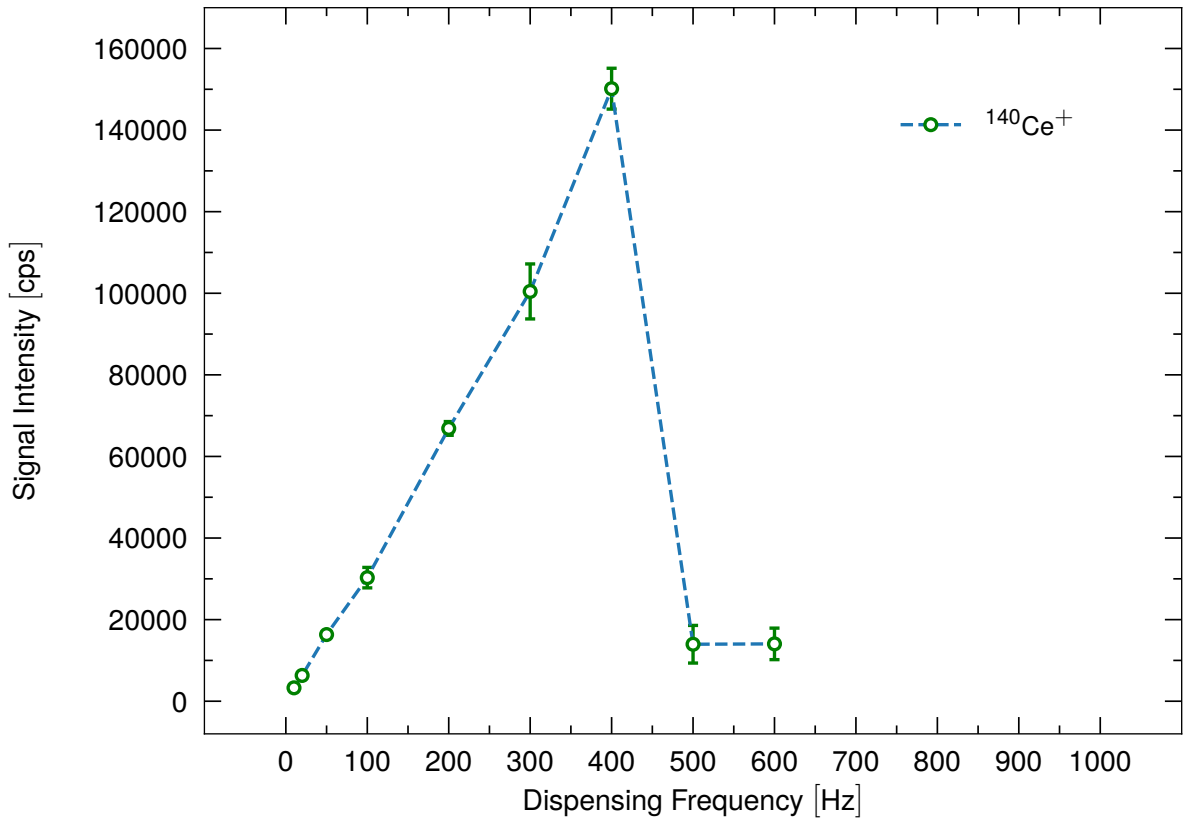

Figure S7 68 μm sized (on average) monodisperse droplets comprising a multi-element solution (20 ppb in 1% HNO_3) were analyzed using the falling tube setup which was mounted on an ICP-TOFMS (icpTOF-2R, Tofwerk AG, Thun, Switzerland) instrument. The following operating conditions were applied: 0 to 0.16 L min^{-1} Ar and 0.44 to 0.71 L min^{-1} He carrier gas, 0.7 L min^{-1} make-up gas Ar, 1550 W ICP power, 15 L min^{-1} plasma gas, 0.8 L min^{-1} auxiliary gas. The signal intensity was correlated with the applied droplet dispensing frequency analogously to **Figure 4**. Here, a horizontally oriented plasma and the falling tube setup were used to detect the dispensed droplets. The gas flows had to be re-adjusted with every change of the dispensing frequency. A linear correlation above 400 Hz was not observed which indicates limited throughput capabilities of the presented setup.

References

1. Koch, J.; Flamigni, L.; Gschwind, S.; Allner, S.; Longerich, H.; Günther, D., Accelerated evaporation of microdroplets at ambient conditions for the on-line analysis of nanoparticles by inductively-coupled plasma mass spectrometry. *J. Anal. At. Spectrom.* **2013,** *28* (11), 1707-1717.
2. Nishiguchi, K.; Utani, K.; Fujimori, E., Real-time multielement monitoring of airborne particulate matter using ICP-MS instrument equipped with gas converter apparatus. *J. Anal. At. Spectrom.* **2008,** *23* (8), 1125-1129.
3. Nishiguchi, K.; Utani, K.; Fujimori, E., Real-time multielement monitoring of airborne particulate matter using ICP-MS instrument equipped with gas converter apparatus. *J. Anal. At. Spectrom.* **2008,** *23* (8).
4. Rumble, J. R., *CRC Handbook of Chemistry and Physics, Online-Ressource*. 101st ed.; 2020.
5. Speight, J. G., *Lange's handbook of chemistry, Online-Ressource*. 16th ed.; McGraw-Hill: New York, 2005.
6. Zhang, Y. M.; Evans, J. R. G.; Yang, S. F., Corrected Values for Boiling Points and Enthalpies of Vaporization of Elements in Handbooks. *J. Chem. Eng. Data* **2011,** *56* (2), 328-337.
7. Tanner, S. D., Characterization of Ionization and Matrix Suppression in Inductively-Coupled Cold-Plasma Mass-Spectrometry. *J. Anal. At. Spectrom.* **1995,** *10* (11), 905-921.
8. Gschwind, S.; Flamigni, L.; Koch, J.; Borovinskaya, O.; Groh, S.; Niemax, K.; Günther, D., Capabilities of inductively coupled plasma mass spectrometry for the detection of nanoparticles carried by monodisperse microdroplets. *J. Anal. At. Spectrom.* **2011,** *26* (6), 1166-1174.